Novel osteoconductive β-tricalcium phosphate/poly(L-lactide-co-e-caprolactone) scaffold for bone regeneration: a study in a rabbit calvarial defect

Pihlman, Hanna[1]
Keränen, Pauli[1]
Paakinaho, Kaarlo[2, 5]
Linden, Jere[1]
Hannula, Markus[3]
Manninen, Iida-Kaisa[4]
Hyttinen, Jari[2]
Manninen, Mikko[5]
Laitinen-Vapaavuori, Outi[1]

1 Faculty of Veterinary Medicine, University of Helsinki, Finland
2 Faculty of Medicine and Life Sciences, Biomeditech, University of Tampere, Finland
3 Faculty of Biomedical Science and Engineering, Tampere University of Technology, Finland
4 Muonio Health Center, Muonio, Finland
5 Orton Orthopaedic Hospital, Helsinki, Finland

Corresponding author
hanna.pihlman@helsinki.fi, phone +358 400459932

Abstract

The advantages of synthetic bone graft substitutes over autogenous bone grafts include abundant graft volume, lack of complications related to the graft harvesting, and shorter operation and recovery times for the patient. We studied a new synthetic supercritical CO_2 –processed porous composite scaffold of β-tricalcium phosphate and poly(L-lactide-co-caprolactone) copolymer as a bone graft substitute in a rabbit calvarial defect.

Bilateral 12 mm diameter critical size calvarial defects were successfully created in 18 rabbits. The right defect was filled with a scaffold moistened with bone marrow aspirate, and the other was an empty control. The material was assessed for applicability during surgery. The follow-up times were 4, 12, and 24 weeks. Radiographic and micro-CT studies and histopathological analysis were used to evaluate new bone formation, tissue ingrowth, and biocompatibility.

The scaffold was easy to shape and handle during the surgery, and the bone-scaffold contact was tight when visually evaluated after the implantation. The material showed good biocompatibility and its porosity enabled rapid invasion of vasculature and full thickness mesenchymal tissue ingrowth already at four weeks. By 24 weeks, full thickness bone ingrowth within the scaffold and along the dura was generally seen. In contrast, the empty defect had only a thin layer of new bone at 24 weeks. The radiodensity of the material was similar to the density of the intact bone.

In conclusion, the new porous scaffold material, composed of microgranular β-TCP bound into the polymer matrix, proved to be a promising osteoconductive bone graft substitute with excellent handling properties.

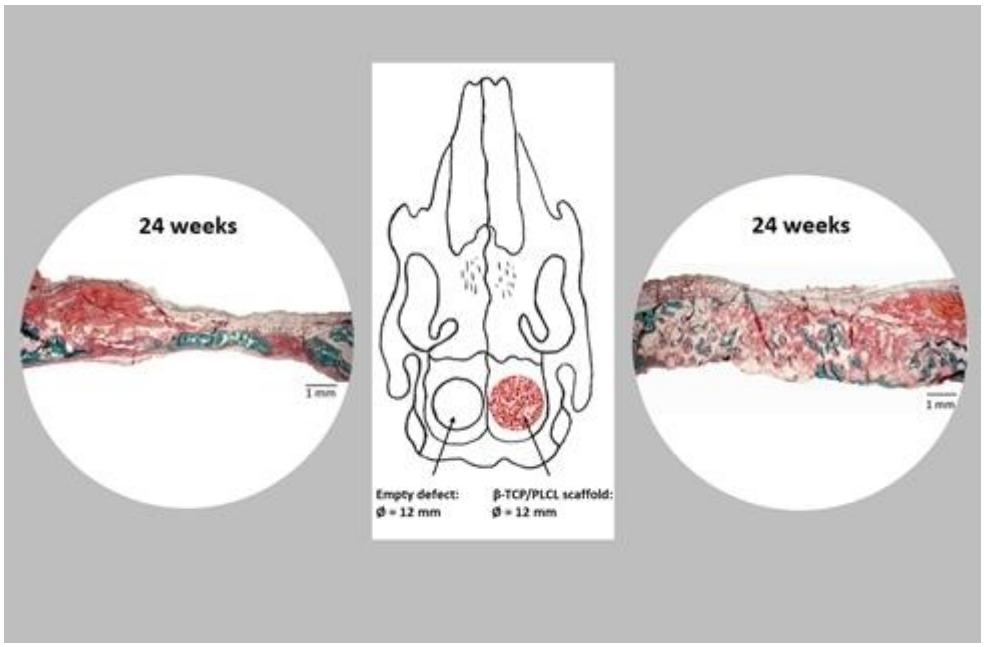

1 Introduction

Large critical size bone defects cannot heal without the osteoinductive or osteoconductive properties of a bone graft or its substitute [1]. Today, autologous bone grafts are considered to be the gold standard since they have good osteoinductive, osteoconductive, and osteogenic properties and induce no rejection in the body of the patient [2-4]. However, autologous bone grafting also has disadvantages, such as donor site pain, nerve or other soft tissue injuries, blood loss or hematoma formation, and also limited graft volume [2, 5-8]. In iliac crest bone graft harvesting procedures, the minor complication rate has varied between 7% and 39% and the major complication rate between 0.8% and 25% [3, 8].

Synthetic bone graft materials have been developed to minimize the complications related to autogenous bone graft harvesting. An optimal bone graft substitute should show good biocompatibility, facilitate tissue ingrowth, and stimulate new bone formation [1, 2]. The biodegradability of the material needs to be on a level where it gives enough structural support but also allows new bone regeneration to replace the decomposing material [1, 2, 9]. Commercially available bone grafts are either brittle ceramics, hard bioactive glass particles, or paste-like fillings [10, 11] that offer limited options in terms of shaping or tailoring the synthetic graft according to operational need.

An option to increase the operational freedom for the surgeon and the resilience of ceramic-based bone graft substitute materials, is to use composite techniques to bind microgranular ceramic particles into a solid form with a biodegradable polymer matrix and to further foam the composite material into a structure that mimics bone. An example of such a structure is a supercritical CO_2 -foamed composite of β-tricalcium phosphate and poly(L-lactide-co-caprolactone) copolymer (β-TCP/PLCL). The ceramic component, β-tricalcium phosphate (β-TCP), shows a similar composition and calcium phosphorus ratio as the mineral phase of native bone. Interestingly, its ability to promote bone healing was demonstrated already a hundred years ago [12]. Recently, the osteoconductive properties and biocompatibility of β-TCP have been shown in experimental and clinical studies [13-15]. β-TCP is mainly degraded in the body by dissolution, but a small amount of degradation is mediated by osteoclasts [16].

The second component, poly(L-lactide-co-ε-caprolactone), is a copolymer of lactide and ε-caprolactone, and its biocompatibility has been demonstrated in various studies [17-19]. The biodegradability of the polymer is based on non-enzymatic hydrolysis [19]. The porous and flexible nature of the β-TCP/PLCL scaffold enables an easy addition of bone marrow aspirate into the scaffold which in turn enhances its osteoinductive and osteogenic properties [11, 20]. Notably, bone marrow aspiration can be done percutaneously, for example, from the iliac crest, which has a significantly lower complication rate when compared with bone graft harvesting from the iliac crest [21].

The main aim of the present study was to evaluate the tissue ingrowth, new bone formation, biocompatibility, and biodegradability of a new β-TCP/PLCL material in a 12 mm critical size calvarial defect in rabbits. In addition, we evaluated the applicability of the material during surgery.

2 Materials and Methods

2.1 β-TCP/PLCL composite scaffold

Bioabsorbable porous composite scaffolds were manufactured by melt-mixing polylactide-co-ε-caprolactone 70L/30CL (PLCL; Purasorb PLC 7015, Corbion Purac Biomaterials, Gorinchem, The Netherlands) and β-tricalcium phosphate (β-TCP; Plasma Biotal Ltd., Buxton, United Kingdom) with the mixing ratio of 50 wt-% of β-TCP in the composite. The

composite rods were foamed by supercritical carbon dioxide into porous composite blocks with the porosity of 65% and an average pore size of 380 µm ± 150 µm measured by µ-CT (MicroXCT-400, Zeiss) with a resolution of 5 µm. After foaming, the blocks were cut into 2.4 mm (± 0.5 mm) thick plates and gamma-irradiated for sterility with a minimum dose of 25 kGy.

2.2 Surgical procedures

The study and surgical protocols were approved by the Finnish Animal Experiment Board (ESAVI/5398/04.10.07/2014). Furthermore, the study complied with Finnish legislation on animal experimentation and the European Union Directive 2010/63/EU. All efforts were taken to minimize the suffering and distress of the rabbits during the study.

A total of twenty female New Zealand White Rabbits aged from 18 to 32 weeks were operated. The rabbits were sedated with subcutaneous injection of medetomidine 0.3 mg/kg (Domitor® 1 mg/mL, OrionPharma) and ketamine 35 mg/kg (Ketador vet® 100 mg/mL, Richter Pharma). All the rabbits received 0.9% sodium chloride with 5% glucose 10 mL/kg/h intravenously during the procedure. Preoperatively, 15 mg/kg trimethoprime-sulfa (Duoprim® 200/40 mg/mL, Intervet International), 4 mg/kg carprophen (Norocarp® 50 mg/mL, Norbrook Laboratories), and 0.03 mg/kg buprenorphine (Bupaq® 0.3 mg/mL, Richter Pharma) were given intravenously. Anesthesia was maintained with 1.5% isoflurane (IsoFlo® vet 100%, Abbott Laboratories) via endotracheal tube or mask. If needed, intravenous boluses of ketamine 10 mg/kg or propofol (Vetofol® 10 mg/mL, Norbrook Laboratories) 2 mg to 5 mg/rabbit were given to effect. The top of the head and the lateral side of the stifle joint were clipped and prepared for aseptic surgery. Strict aseptic surgical protocols were followed during the procedure.

A midline sagittal skin incision was made from behind the ears to the level of the first cervical vertebrae. The periosteum was incised from the midline and elevated to reveal the bone surface of the parietal bones. A custom-made 12 mm diameter trephine was used to mark the round defects on both parietal bones. Bicortical craniotomy was made by using a 2.5 mm and 4 mm diameter burr with continuous saline irrigation [Electric Pen Drive (EPD), DePuy Synthes].

During the operation, scaffold plates were press-cut into 12 mm diameter discs with a trephine from prefabricated oversized plates. Bone marrow aspirate was collected with a 2 cc syringe and 21 G needle from a 3.2 mm diameter monocortical drill hole in the lateral femoral condyle and used for moistening the scaffold. Moistening was performed by squeezing the scaffold in a sterile elastic pouch filled with aspirate so that the porous structure would be fully moistened. The bone marrow aspirate was used to promote osteogenic and osteoinductive properties. The right defect was filled with scaffold by bending it along the shape of the skull. The left one served as an empty control. The surgical field was then flushed with saline before closure. The periosteum and the skin were closed in layers with 4-0 poliglecaprone 25 (Monocryl®, Ethicon).

Postoperatively, a subcutaneous injection of atipametzole (Antisedan® 5 mg/mL, OrionPharma) was given. For control of postoperative pain, the rabbits received a subcutaneous injection of buprenorphine 0.03 mg/kg two to three times a day for three days and carprophen 4 mg/kg once a day for two days. The rabbits also received a subcutaneous injection of metoclopramide 0.2 mg/kg (Primperan® 5 mg/mL, Sanofi) to increase the intestinal motility twice a day for one day. Hay and water were freely available. After two weeks of restricted cage rest, the rabbits were removed to a large group housing area.

Two rabbits were lost at the early stage of the experiment and were excluded from the follow-up studies. One rabbit had a cardiac arrest at the end of the surgical procedure, and the other one was lost three days after the operation. In post

mortem necropsy, an injury in the left hemisphere of the cerebral cortex was found.

2.3 Applicability of the scaffold

The applicability of the scaffold was subjectively evaluated by the surgeons during the surgical procedures. The focus was on intraoperative shaping of the scaffold, possible crumbling of the scaffold during handling, the ability to fully moisten the scaffold with the bone marrow aspirate harvested from the femoral condyle, the ability to fill the defect, and visual evaluation of the bone-scaffold interface. The bone-scaffold interface was evaluated to ascertain whether the contact between the scaffold and bone was tight or not.

2.4 Specimen collection

The 18 rabbits were randomly divided in groups of six animals and euthanized 4, 12, and 24 weeks after the surgery. Euthanasia was performed with subcutaneous injection of 0.3 mg/kg medetomidine and 35 mg/kg ketamine followed by intracardiac injection of pentobarbital 300 mg/rabbit (Mebunat vet 60 mg/mL, Orion Pharma). The parietal bone blocks including the defects and the intact bone around them were harvested with an EPD diamond coated circular burr.

2.5 Radiographic examination

After the surgical procedure, a dorsoventral radiograph (Practix 400, Philips, 46 kV and 4.0 mAs) of the skull was taken. The radiographs were used to evaluate the location of the defects and the radiographic opacity of the scaffold.

After euthanasia, the harvested bone blocks were radiographed. A dorsoventral projection (46 kV, 4.0 mAs) of the skull was taken. The new bone formation in the empty defect was subjectively evaluated as no new bone formation, a small amount of new bone formation, or obvious new bone formation. Possible fractures, cyst formation, an excessive amount of callus or signs of osteomyelitis were recorded.

2.6 Micro-CT imaging

A micro-CT study (MicroXCT-400, Zeiss, Pleasanton, CA, USA) was performed on all of the harvested bone blocks before histologic preparation. A tube voltage of 110 kV and a tube current of 91 μA were selected. From each sample, 1600 projections were taken with a 19.97 x 19.97 x 19.97 μm voxel size. Exposure time was 4 seconds. Projections were reconstructed with the manufacturer's XMReconstructor software. Image processing and analysis were done with Avizo Software (Thermo Fisher Scientific, Waltham, MA, USA).

2.6.1 Total amount of radiodense material

The total amount of radiodense material from the scaffold filled defect and the empty defect was assessed from the micro-CT images. A 12 mm in diameter and 4 mm in height cylinder shaped area was manually placed on the center of the defect and used as a volume of interest for the assessment.

2.6.2 Distribution of radiodense material

Radiodense material distribution over the defects was evaluated with a novel method (Fig. 1). To create the distribution map, a 3D-image of the skull was flattened to the 2D-image where one pixel represented a column of voxels in a 3D-picture. Each rabbit had its own individual radiodensity scale where 0 was air and 1 was mean radiodensity of the intact calvarian bone around the defect. Each pixel in the 2D-picture had the same radiodensity as the highest value in the 3D-picture voxel column. Eleven measurement lines per defect were measured from the 2D-picture. The length of the measurement line was 14 mm. There were 100 measurement points in each measurement line. Those measurement point areas covered an area of 100 x 1000 µm, and the radiodensity of that area was the mean radiodensity of the all pixels in that area. A total of 1100 measurements per defect were measured. There were 40 µm cap between the measured areas in the measurement lines. Otherwise, the measured areas were in contact with each other. MathLab (The MathWorks, Inc., Natick, MA, USA) was used to create a graph of the mean radiodensities in each follow-up group (Fig. 2).

2.7 Histological analysis

The harvested bone blocks were fixed in 10% buffered formalin, dehydrated in ascending alcohol series, and embedded in methyl methacrylate (MMA). Then, 5 µm thin slices were sectioned from the midline of the defect using a hard tissue microtome (Leica, SM2500) and stained employing Weigert Van Gieson (WVG) and Masson-Goldner Thrichrome (MT) methods.

The evaluation of the biocompatibility of the scaffold included the subjective grading of implant decomposition, osteogenesis, and histiocytic reaction on the surface of the implant using a four-tier scale (+/- = minimal, + = mild, ++ = moderate and +++ = marked). A descriptive histopathological analysis of the empty defects was then performed.

2.8 Statistical analyses

A Kolmogorov-Smirnov test was used to test the normal distribution of the data. Mann-Whitney test was used to compare groups at different follow-up times. Bonferroni correction was used. Wilcoxon Signed Rank test was used to compare scaffold groups with the empty defect groups. The tests were two-tailed. A p-value under 0.05 was considered as statistically significant. IMB SPSS (version 23, Armonk, NY, USA) was used for the statistical analyses.

3 Results

3.1 Applicability of the scaffold

At room temperature, the scaffold material was relatively rigid and easy to cut with a trephine. During handling, however, the material temperature increased close to body temperature, and thereby its elasticity was increased. The increased elasticity of the material enabled easy impregnation of bone marrow aspirate. Furthermore, due to the elasticity of the scaffold, it was easily squeezed and bent into the defect. Therefore, the convex shape of the lateral side of the skull did not complicate the implantation or influence bone scaffold contact. In all scaffold filled defects, the bone-scaffold contact in the interface was tight when visually evaluated after the implantation. No visible particle loosening from the scaffold occurred during the press-cut, during the moistening of the scaffold in a squeezing bag, or during the implantation.

3.2 Radiographic examination

During the postoperative radiographic examination, the scaffold could not be distinguished from the skull bones in any of the radiographs. The empty defect was visible in 3 out of 18 (17%) rabbits due to a summation of other calvarial structures.

In post-mortem radiographs from the parietal bone blocks, the density of the scaffold-filled defects was comparable with the density of the intact skull next to the defect. The only visible change in the scaffold side was that the structure of the scaffold turned from homogenous to more heterogenous and grainy during the follow-up period. Excessive callus formation, signs of osteomyelitis, or bone cyst formation were not seen in any scaffold-filled defects during the whole study period.

In post mortem radiographs from the bone blocks, the radiodensity of the empty defect increased with time. At 4 weeks, 2 out of 6 defects showed no new bone formation, two had a small amount of new bone formation, and two had obvious new bone formation. At 12 weeks, 2 out of 6 defects showed a small amount of new bone formation, and four had obvious new bone formation. At 24 weeks, all six defects showed obvious new bone formation. Despite the new bone formation, the empty defects in all groups were apparent, and the radiodensity was lower than the density of the scaffold-filled defects or the intact skull next to the defects.

3.3 MicroCT imaging

Typical micro-CT images of bone growth from the scaffold-filled and empty defects are shown in Figure 3.

3.3.1 Total amount of radiodense material

The total amount of radiodense material in the 12 mm calvarian defects analyzed by micro-CT from the volumes of interest are presented in Table 1. The defects filled with β-TCP/PLCL composite scaffold had a similar level of radiodensity at 4 and 12 weeks (31.6% and 30.1%, respectively). However, the total amount of radiodense material decreased significantly ($p = 0.03$) by 22.4% between weeks 12 and 24.

In the empty defects, the radiodense material filled 7.5% of the volume of interest at 4 weeks increasing up to 11.0% and 11.4% at 12 and 24 weeks, respectively. The changes in the amounts of radiodense material were not, however, statistically significant between any of the groups.

The total amount of radiodense material was significantly ($p = 0.028$) higher throughout the follow-up times in the scaffold-filled defects compared with the empty defects.

3.3.2 Distribution of radiodense material

The distribution graph of radiodense material in the scaffold-filled and empty defects presented in Figure 2 shows that the mean radiodensity of the scaffold-filled defects was maintained close to the radiodensity of an intact skull throughout the defect in all groups. Slightly lower radiodensities were seen at 24 weeks.

In the empty defects, the mean radiodensity was lower than that of the intact skull. The radiodensity inside the defects

near the edge increased at 12 and 24 weeks, and at 24 weeks also in the middle of the defects.

3.4 Histologic evaluation

Already at 4 weeks, tissue reaction to the scaffold consisted of a network of tissue trabeculae advancing from the bone walls of the defect into the porous material. The trabeculae were composed of an abundant vascular network, mesenchymal cells with a moderate number of multinucleated giant foreign body cells and macrophages, and even included some small woven bone nidi surrounded by osteoid. In addition, loose cell strands and erythrocytes admixed with the scaffold (Fig. 4a).

At 12 and 24 weeks, the trabeculae exhibited a mesenchymal core, occasionally showing osteoblast differentiation and variable vascularization as well as small to moderate-sized woven bone spicules and nidi surrounded by osteoid. The trabeculae were flanked by moderate to marked histiocytic reaction with ample macrophages and multinucleated giant foreign body cells (Table 3; Fig. 4a). At 12, and especially at 24 weeks, osteogenesis proceeded variably along the dural and superficial periosteum further to the trabeculae.

Based on histology, the scaffolds showed moderate to marked decomposition already at 4 weeks, further advancing from 12 to 24 weeks. At 12 weeks, the scaffold material was actively degraded, and the scaffold area appeared to be reduced to approximately 50%. At 24 weeks, macrophages and multinucleated giant cells continued to be abundant and the scaffold area reduced, pointing to progressing histological decomposition (Table 3; Fig. 4a).

The empty defects seemed to regenerate by intramembranous ossification, osteogenesis mainly proceeding along the dural periosteum (Fig. 4b). At 4 weeks, small mineralized bone islands, osteoid and highly vascularized connective tissue spanned over the defect. At 12 and 24 weeks, mineralized bone with a thin osteoid rim covered approximately 30% to 60% of the length of the defect but remained substantially thinner than intact calvarial bone. Notably, muscle and adipose tissue bulged into the defect from the skull surface (Fig. 4b).

4 Discussion

In our study, the new β-TCP/PLCL scaffold showed osteoconductive properties as previously demonstrated on pure β-TCP granules in calvarial defects of several different species [22-24]. Osteoconductive materials are recommended to be used in conjunction with bone marrow aspirate or with a bone graft, creating material with osteoconductive, osteoinductive, and osteogenic properties [11, 20]. Bone marrow aspirate was used in this study to improve the properties of the osteoconductive material. Mineralized bone and osteoid were not only seen along the scaffold but also inside the scaffold increasingly at all follow-up times. This ability to promote three-dimensional tissue regeneration can most likely be explained by the high porosity of the scaffold (65%), and an average pore size (380 μm) that mimics that of cancellous bone [25]. Previously, Tsuruga et al. [26] showed that an average pore size larger than 300 μm results in higher osteogenesis than smaller pore sizes. In our study, the high porosity and optimal pore size enabled effective vascularization and mesenchymal tissue ingrowth throughout the scaffold already at 4 weeks. The vascularization and thus high oxygenation is needed for tissue ingrowth and new bone formation [27]. A considerable amount of mesenchymal tissue inside the scaffold was also seen at all follow-up times. This is also a relevant finding since the mesenchymal tissue has been shown to have the ability to differentiate into bone tissue [16].

During surgery, the moldable β-TCP/PLCL scaffold filled the whole bony defect and seemed to give structural support.

This was confirmed in histology since the surrounding muscles and adipose tissues did not invade into the defect. This is an important finding because soft tissues bulging into the defect significantly hinder the bone regeneration process [28]. This was also apparent in the empty defects in this study, where bulging of soft tissues occupied the space and only a thin layer of new bone followed the dural periosteum. This finding is in accordance with previous studies where in calvarial defects new bone formation along the dura is reported to be the principal regeneration type [28, 29]. Notably, the scaffold-filled defects also exhibited pronounced dural osteogenesis in addition to bone ingrowth into the porosity of the scaffold, and new bone formation appeared to slow down from 12 to 24 weeks. It is thus possible that the degradation of the material was not fast enough from 4 to 24 weeks to enable enough space for accelerated new bone formation inside the scaffold. Accordingly, new bone formation in scaffolds has been shown to be slower than in β-TCP granule-filled defects because the material decreases the space available for new bone formation [24, 29, 30]. On the other hand, fast degradation of a filling material may lead to premature loss of structural support, and therefore may not lead to desirable or faster new bone formation. Further studies are needed to see the effect of material degradation on bone formation with longer follow-up times.

In our study, the rapid invasion of vasculature, mesenchymal tissue, and bone implied that the biocompatibility of the material was good with no signs of adverse reactions, such as purulent inflammation, necrosis or fibrosis around the scaffold material. Typical foreign body reaction with histiocytes, macrophages, and multinucleated giant cells was observed at all time points, especially at 12 and 24 weeks. This reaction is associated with the degradation process of the scaffold and is seen with other materials, such as hydroxyapatite and β-TCP [15, 31-33].

The drawback with existing synthetic ceramic or bioactive glass scaffolds is their brittle and hard nature [10, 34]. Thus, the intraoperative molding or shaping of these materials is usually difficult [34] and pure ceramics may create excessive stress on the surrounding tissues during implantation and may even cause fissures to the bone cortex [35]. The cohesion between the tissues and pure ceramics is also lower than the cohesion of autografts, which might cause particles to spread around the surgical field during implantation [35, 36]. Grafting near the joints might cause loose particles to migrate between joint surfaces, and thus create third-body wear [37]. In our study, the new β-TCP/PLCL scaffold was easily moldable and adaptable to the anatomical convex contour of the skull, even though the ceramic concentration of the scaffold was 50 weight-%. Because of its elasticity, the scaffold could be compressed during implantation, and it could also be fitted tightly into the defect. There was no visible ceramic particle loosening from the scaffold at any stage of the procedure, i.e., during moistening of the scaffold with the marrow aspirate in a squeezing pouch or during implantation.

As shown in a canine calvarial model, pure β-TCB has higher radiodensity than intact bone, and thus the implant area can be easily distinguished from the bone tissue [23]. In this study, the mixture of micro-granule β-TCB and PLCL-polymer produced a composite material with a very similar radiodensity to intact calvarial bone in the radiographs. In fact, the radiodensities of the bone and the scaffold materials were so similar that it was not possible to differentiate them from each other in the micro-CT study. The textural change of the scaffold from homogenous to grainier and heterogenous during the follow-up period was probably due to scaffold degradation and tissue ingrowth. The total amount of radiodense material and the mean radiodensity analyzed by micro-CT, was affected by the non-dissolved β-TCP microgranules in the scaffold-filled defects, and therefore the analysis result is a combination of new bone and the ceramic phase of the scaffold. Sanda et al. [38] reported a similar amount of radiodense material in both 4- and 8-week groups in rabbits with an 8 mm diameter calvarial defect filled with pure β-TCB granules. In their study, histomorphometric analysis confirmed that there was no mass loss of TCP during the 8 weeks. In our study, the decrease of radiodense material in the scaffold-filled defect started between 12 and 24 weeks. This finding is in accordance with the histological evaluation.

A 15 mm diameter defect has been classically defined as a critical size defect in a rabbit calvarial [39]. The new bone formation will plateau after 12 weeks in a 15 mm calvarial defect [24, 40, 41]. In this study, a significant increase in new bone formation after 4 weeks was not observed and the total amount of radiodense material in the empty defects plateaued to approximately 11%. Correspondingly, histopathology confirmed that new bone formation proceeded only as a thin layer or islands accompanying the dura. Nowadays, an alternative definition for critical size defect is a defect that will not spontaneously heal during the time of the experiment [28], and therefore smaller defects have also been used in various calvarial defect studies [42-44]. The findings of this study support this definition, and therefore a 12 mm calvarial defect can be considered as a critical size defect in this study.

5 Conclusion

This study presented the potentiality of a new supercritical CO_2-foamed poly(L-lactide-co-caprolactone) copolymer β-tricalcium phosphate composite scaffold in three-dimensional tissue regeneration in a critical sized rabbit calvarial defect model. β-TCP was successfully utilized in the scaffold to provide an osteoconductive surface for bone ingrowth, and the interconnected pore structure enabled abundant vascularization and full thickness tissue ingrowth throughout the material. The resilient composite structure could be cut to shape and compressed into the bone defect. As a result, the composite scaffold was easier to use and more versatile than most of the available products used for bone regeneration.

Acknowledgements

This study was financially supported by the Finnish Funding Agency for Technology and Innovation (40326/13) and by grants from the Finnish Foundation of Veterinary Research and The Finnish Veterinary Foundation. The authors kindly acknowledge DVM Mikael Morelius for the help with surgical procedures.

Compliance with ethical standards

Conflict of interest

The authors declare that they have no conflict of interest.

References

1. Calori GM, Mazza E, Colombo M, Ripamonti C. The use of bone-graft substitutes in large bone defects: Any specific needs? Injury. 2011;42:56–63.

2. Moore WR, Graves SE, Bain GI. Synthetic bone graft substitutes. ANZ J Surg. 2001;71:354–61.

3. Myeroff C, Archdeacon M. Autogenous bone graft: donor sites and techniques. J Bone Joint Surg. 2011;93:2227–36.

4. Fillingham Y, Jacobs J. Bone grafts and their substitutes. Bone Join J. 2016;98:B(1 Suppl A):6–9.

5. Schnee CL, Freese A, Weil RJ, Marcotte PJ. Analysis of harvest morbidity and radiographic outcome using autograft for anterior cervical fusion. Spine. 1997;22:2222–7.

6. Sawin PD, Traynelis VC, Menezes AH. A comparative analysis of fusion rates and donor-site morbidity for autogeneic rib and iliac crest bone grafts in posterior cervical fusions. J Neurosurg. 1998;88:255–65.

7. Ebraheim NA, Elgafy H, Xu R. Bone-graft harvesting from iliac and fibular donor sites: techniques and complications. J Am Acad Orthop Surg. 2001;9:210–8.

8. Dimitriou R, Mataliotakis GI, Angoules AG, Kanakaris NK, Giannoudis PV. Complications following autologous bone graft harvesting from the iliac crest and using the RIA: A systematic review. Injury. 2011;42:3–15.

9. Bizenjima T, Takeuchi T, Seshima F, Saito A. Effect of poly(lactide-co-glycolide) (PLGA)-coated beta-tricalcium phosphate on the healing of rat calvarial bone defects: a comparative study with pure-phase beta-tricalcium phosphate. Clin Oral Implants Res. 2016;27:1360–7.

10. Hak DJ. The use of osteoconductive bone graft substitutes in orthopaedic trauma. J Am Acad Orthop Surg. 2007;15:525–36.

11. Thaler M, Lechner R, Gstöttner M, Kobel C, Bach C. The use of beta-tricalcium phosphate and bone marrow aspirate as a bone graft substitute in posterior lumbar interbody fusion. Eur Spine J. 2013;22:1173–82.

12. Albee FH. Studies in bone growth: Triple calcium phosphate as a stimulus to osteogenesis. Ann Surg. 1920;71:32–9.

13. Zerbo IR, Zijderveld SA, de Boer A, Bronckers AL, de Lange G, ten Bruggenkate CM, et al. Histomorphometry of human sinus floor augmentation using a porous beta-tricalcium phosphate: a prospective study. Clin Oral Implants Res. 2004;15:724–32.

14. Zijderveld S, Zerbo I, van den Bergh J, Schulten E, ten Bruggenkate C. Maxillary sinus floor augmentation using a β-tricalcium phosphate (Cerasorb) alone compared to autogenous bone grafts. Int J Oral Maxillofac Implants. 2005;20:432–40.

15. Ghanaati S, Barbeck M, Orth C, Willershausen I, Thimm BW, Hoffmann C, et al. Influence of β-tricalcium phosphate granule size and morphology on tissue reaction in vivo. Acta Biomater. 2010;6:4476–87.

16. Zerbo IR, Bronckers AL, de Lange G, Burger EH. Localisation of osteogenic and osteoclastic cells in porous β-tricalcium phosphate particles used for human maxillary sinus floor elevation. Biomaterials. 2005;26:1445–51.

17. Honda M, Yada T, Ueda M, Kimata K. Cartilage formation by cultured chondrocytes in a new scaffold made of poly(L-lactide-ϵ-caprolactone) sponge. J Oral Maxillofac Surg. 2000;58:767–75.

18. Honda M, Morikawa N, Hata K, Yada T, Morita S, Ueda M, et al. Rat costochondral cell characteristics on poly (l-lactide-co- ε-caprolactone) scaffolds. Biomaterials. 2003;24:3511–9.

19. Jeong SI, Kim SH, Kim YH, Kim B, Kang SW, Kwon JH, et al. In vivo biocompatibilty and degradation behavior of elastic poly(l-lactide- co- ε-caprolactone) scaffolds. Biomaterials. 2004;25:5939–46.

20. Nandi SK, Roy S, Mukherjee P, Kundu B, De DK, Basu D. Orthopaedic applications of bone graft & graft substitutes: a review. Indian J Med Res. 2010;132:15–30.

21. Hernigou P, Desroches A, Queinnec S, Flouzat Lachaniette C, Poignard A, Allain J, et al. Morbidity of graft harvesting versus bone marrow aspiration in cell regenerative therapy. Int Orthop. 2014;38:1855–60.

22. Luvizuto ER, Queiroz TP, Margonar R, Panzarini SR, Hochuli-Vieira E, Okamoto T, et al. Osteoconductive properties of β-tricalcium phosphate matrix, polylactic and polyglycolic acid gel, and calcium phosphate cement in bone defects. J Craniofac Surg. 2012;23:e430–3.

23. Tanuma Y, Matsui K, Kawai T, Matsui A, Suzuki O, Kamakura S, et al. Comparison of bone regeneration between octacalcium phosphate/collagen composite and β-tricalcium phosphate in canine calvarial defect. Oral Surg Oral Med Oral Pathol Oral Radiol. 2013;115:9–17.

24. Lappalainen O, Karhula S, Haapea M, Kyllönen L, Haimi S, Miettinen S, et al. Bone healing in rabbit calvarial critical-sized defects filled with stem cells and growth factors combined with granular or solid scaffolds. Childs Nerv Syst. 2016;32:681–8.

25. Hernandes CJ. Cancellous bone. In: Murphy W, Black J, Hastings G, editors. Handbook of biomaterial properties. New York: Springer-Verlag; 2016. pp 15–21.

26. Tsuruga E, Takita H, Itoh H, Wakisaka Y, Kuboki Y. Pore size of porous hydroxyapatite as the cell-substratum controls BMP-induced osteogenesis. J Biochem. 1997;121:317–24.

27. Karageorgiou V, Kaplan D. Porosity of 3D biomaterial scaffolds and osteogenesis. Biomaterials. 2005;26:5474–91.

28. Gosain AK, Santoro TD, Song L, Capel CC, Sudhakar PV, Matloub HS. Osteogenesis in calvarial defects: contribution of the dura, the pericranium, and the surrounding bone in adult versus infant animals. Plast Reconstr Surg. 2003;112:515–27.

29. Lappalainen O, Karhula SS, Haapea M, Kauppinen S, Finnilä M, Saarakkala S, et al. Micro-CT analysis of bone healing in rabbit calvarial critical-sized defects with solid bioactive glass, tricalcium phosphate granules or autogenous bone. J Oral Macillofac Res. 2016;7:e4.

30. Jan A, Sándor G, Brkovic B, Peel S, Kim YD, Xiao W, et al. Effect of hyperbaric oxygen on demineralized bone matrix and biphasic calcium phosphate bone substitutes. Oral Surg Oral Med Oral Pathol Oral Radiol Endod. 2010;109:59–66.

31. Ghanaati S, Barbeck M, Willershausen I, Thimm B, Stuebinger S, Korzinskas T, et al. Nanocrystalline hydroxyapatite bone substitute leads to sufficient bone tissue formation already after 3 months: Histological and histomorphometrical analysis 3 and 6 months following human sinus cavity augmentation. Clin Implant Dent Relat Res. 2013;15:883–92.

32. Miron RJ, Zohdi H, Fujioka-Kobayashi M, Bosshardt DD. Giant cells around bone biomaterials: Osteoclasts or multi-nucleated giant cells? Acta Biomater. 2016;46:15–28.

33. Barbeck M, Booms P, Unger R, Hoffmann V, Sader R, Kirkpatrick CJ, et al. Multinucleated giant cells in the implant bed of bone substitutes are foreign body giant cells – New insights into the material-mediated healing process. J Biomed Mater Res A. 2017;105:1105–11.

34. Peltola M, Kinnunen I, Aitasalo K. Reconstruction of orbital wall defects with bioactive glass plates. J Oral Macillofac Surg. 2008;66:639–46.

35. van Haaren EH, Smit TH, Phipps K, Wuisman PI, Blunn G, Heyligers IC. Tricalcium-phosphate and hydroxyapatite bone-graft extender for use in impaction grafting revision surgery. J Bone Joint Surg [Br]. 2005;87:267–71.

36. Oakley J, Kuiper JH. Factors affecting the cohesion of impaction bone graft. J Bone Joint Surg [Br]. 2006;88:828–31.

37. Schroeder C, Grupp T, Fritz B, Schilling C, Chevalier Y, Utzschneider S, et al. The influence of third-body particles on wear rate in unicondylar knee arthroplasty: a wear simulator study with bone and cement debris. J Mater Sci Mater Med. 2013;24:1319–25.

38. Sanda M, Shiota M, Fujii M, Kon K, Fujimori T, Kasugai S. Capability of new bone formation with a mixture of hydroxyapatite and beta-tricalcium phosphate granules. Clin Oral Implants Res. 2015;26:1369–74.

39. Schmitz JP, Hollinger JO. The critical size defect as an experimental model for craniomandibulofacial nonunions. Clin Orthop Relat Res. 1986;205:299–308.

40. Fok T, Jan A, Peel S, Evans AW, Clokie C, Sándor G. Hyperbaric oxygen results in increased vascular endothelial growth factor (VEGF) protein expression in rabbit calvarial critical-sized defects. Oral Surg Oral Med Oral Pathol Oral Radiol Endod. 2008;105:417–22.

41. Jan A, Sándor G, Iera D, Mhawi A, Peel S, Evans AW, et al. Hyperbaric oxygen results in an increase in rabbit calvarial critical sized defects. Oral Surg Oral Med Oral Pathol Oral Radiol Endod. 2006;101:144–9.

42. Cooper GM, Mooney MP, Gosain AK, Campbell PG, Losee JE, Huard J. Testing the critical size in calvarial bone defects: revisiting the concept of a critical-size defect. Plast Reconstr Surg. 2010;125:1685–92.

43. Borie E, Fuentes R, del Sol M, Oporto G, Engelke W. The influence of FDBA and autogenous bone particles on regeneration of calvaria defects in the rabbit: A pilot study. Ann Anat. 2011;193:412–7.

44. Pelegrine AA, Aloise AC, Zimmermann A, Mello e Oliveira R, Ferreira LM. Repair of critical-size bone defects using bone marrow stromal cells: a histomorphometric study in rabbit calvaria. Part I: Use of fresh bone marrow or bone marrow mononuclear fraction. Clin Oral Implants Res. 2014;25:567–72.

452
453

Table 1. The total amount of radiodense material in the defects measured using micro-CT. The volume of interest was a 12 mm in diameter and 4 mm in height cylinder-shaped area centered in the middle of the defect. SD = standard deviation.

	Scaffold-filled defect			Empty defect		
	N	Mean (SD)	*p*- values	N	Mean (SD)	*p*- values
4 weeks	6	31.6% (2.83)	1.011 (4 vs 12)	6	7.5% (3.23)	0.165 (4 vs 12)
			0.12 (4 vs 24)			0.165 (4 vs 24)
12 weeks	6	30.1% (2.24)	**0.03** (12 vs 24)	6	11.0% (1.30)	2.247 (12 vs 24)
24 weeks	6	22.4% (5.19)		6	11.4% (1.58)	

454
455
456
457

Table 2. Osteogenesis, histiocytic reaction on scaffold surface and scaffold decomposition were graded using a scale from +/- to +++. Number of animals per group was 6.

	+/-, slight	+, mild	++, moderate	+++, marked
Osteogenesis				
4 weeks	4/6	2/6		
12 weeks	2/6	3/6	1/6	
24 weeks	1/6	4/6	1/6	
Histiocytic reaction				
4 weeks		3/6	3/6	
12 weeks				6/6
24 weeks			2/6	4/6
Implant decomposition				
4 weeks			6/6	
12 weeks			2/6	4/6
24 weeks				6/6

458
459

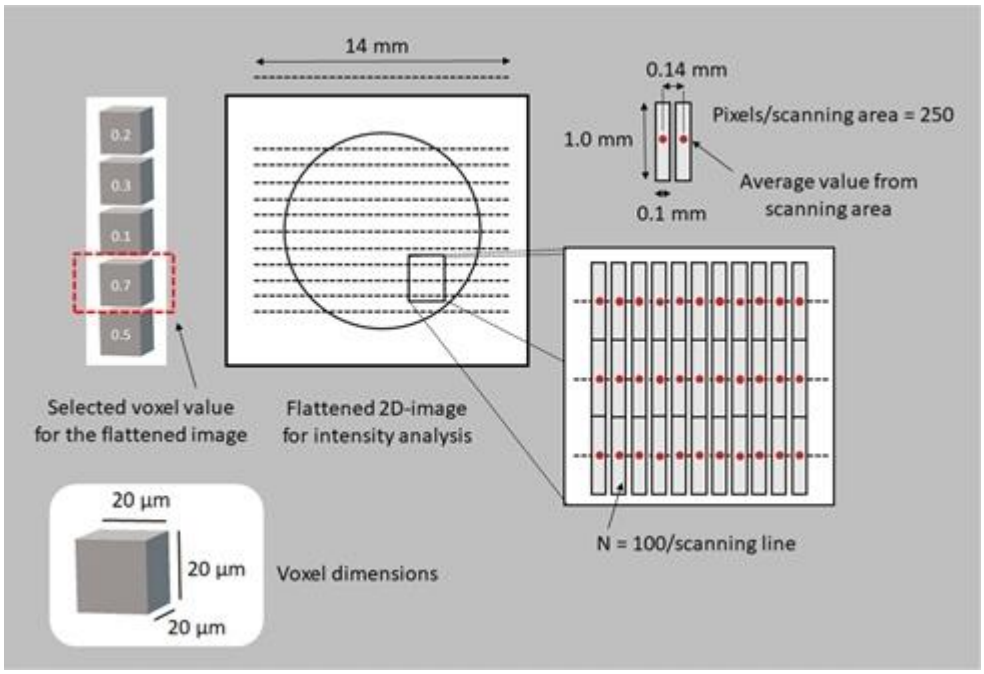

Fig. 1

Method for the radiodensity of the defect. A 2D-figure was created based on the highest radiodensity of a voxel column in a 3D-picture. There were 11 measurement lines going along the defect. In each measurement line, there were 100 measurement areas. Each measurement area was given the value of a mean radiodensity of the 250 pixels in the area.

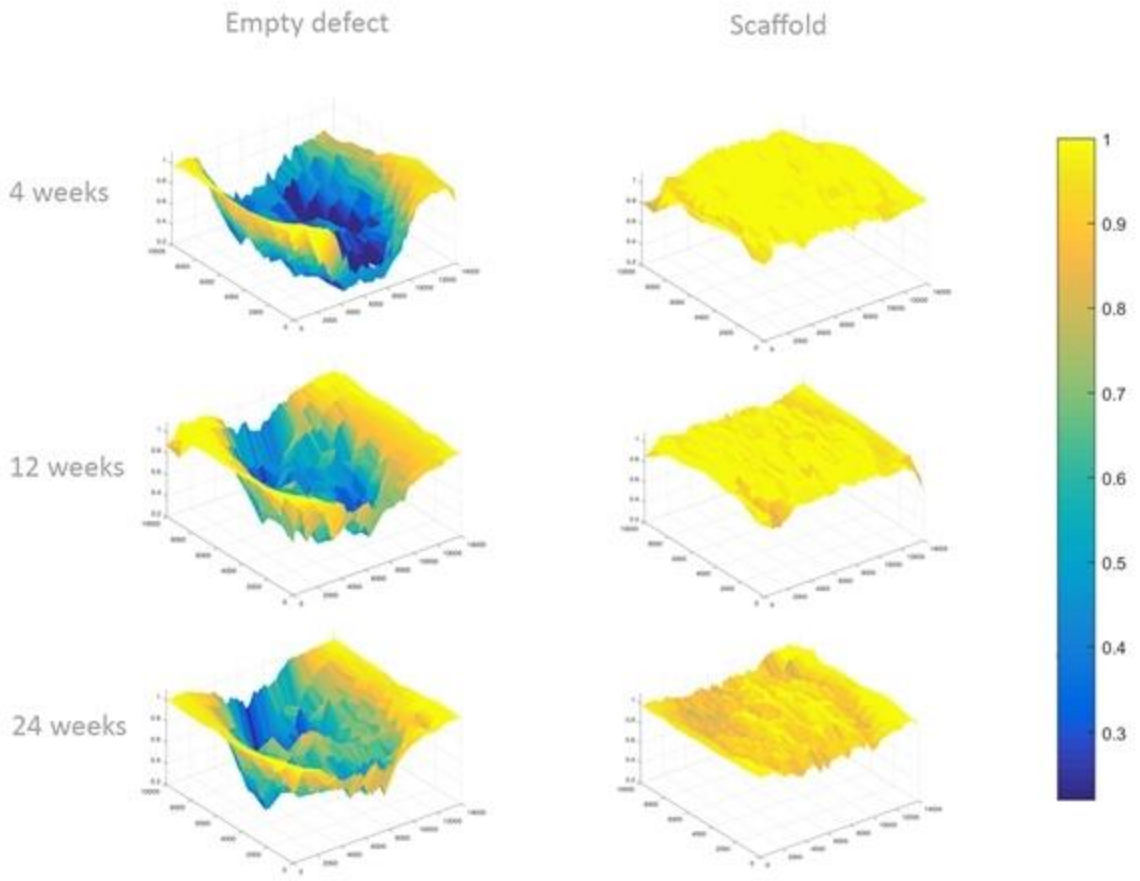

Fig. 2

Mean radiodensities of the defects at 4, 12, and 24 weeks (n = 6). In this analysis, 1 (yellow) is the radiodensity of the intact skull, and 0 (blue) is the radiodensity of the air. The scaffold-filled area has visually similar radiodensities at the follow-up times. At 24 weeks, a small decrease in the radiodensity of the scaffold-filled defect (defect turning from yellow to orange) is seen. In the empty defect, the mean radiodensity is lower than the density of an intact skull. Radiodensity increase inside the defect around the edges at 12 and 24 weeks and also in the middle of the defect at 24 weeks.

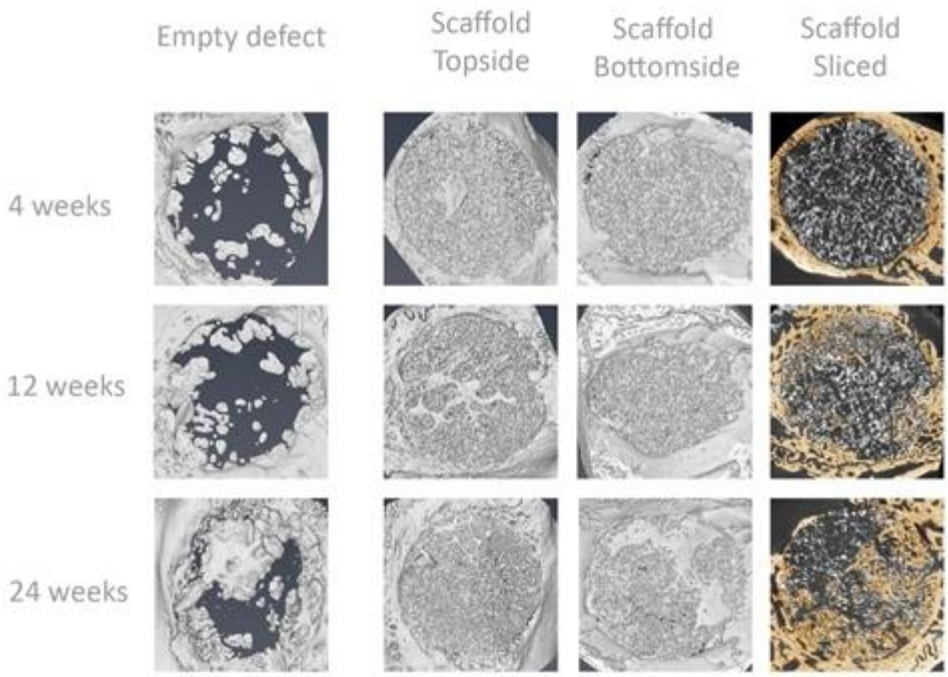

Fig. 3

Micro-CT image from different animals at 4, 12, and 24 weeks. In the empty defect there are small islands of bone inside the defect. Pictures from the top and bottom side and also in the middle of the defect show typical bone regeneration at different times in the scaffold-filled defects. Bone has been manually colored to yellow in the sliced picture. The new bone formation is advancing along the dura and periosteum, but advanced new bone formation inside of the scaffold was seen when the follow-up time increased. The scaffold-bone interface looked tight in all groups.

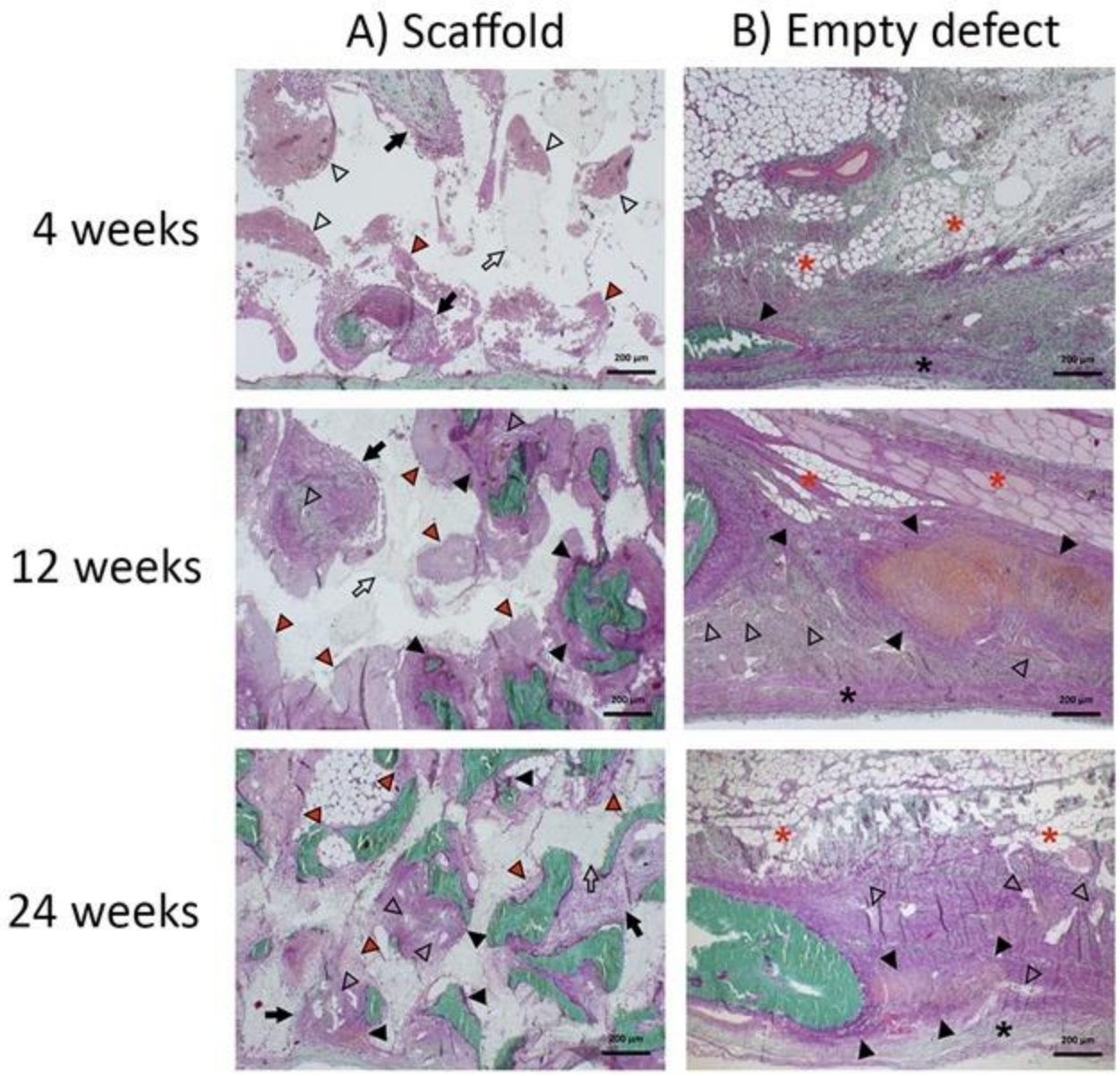

Fig. 4

A: Histology of the bone regeneration, ingrowth into the scaffold and typical tissue reactions at 4, 12, and 24 weeks. At 4 weeks, the scaffold is invaded by mesenchymal cell strands (arrows), ample vasculature/erythrocytes (open arrow heads), and some multinucleated giant cells (red arrow heads). Lacy to opalescent scaffold material (open arrows) is poorly discernible. At 12 and 24 weeks, invading tissue trabeculae show mesenchymal core and variable vascularization as well as mineralized bone islands (green) surrounded by osteoid (closed arrow heads). The trabeculae are flanked by moderate to marked histiocytic reaction with large multinucleated giant cells. **B**: Histology of the empty defects at 4, 12, and 24 weeks. The empty defects regenerate by intramembranous ossification, osteogenesis mainly proceeding along the dural periosteum (asterisk) showing mineralized bone islands, osteoid/ossifying mesenchyme (closed arrow heads) in vascularized connective tissue. Muscle and adipose tissue (red asterisks) bulge into the defect. MT stain, objective magnification 5x.